Inorganic Chemistry

Article

pubs.acs.org/IC

Resonance Raman, Electron Paramagnetic Resonance, and Density Functional Theory Calculations of a Phenolate-Bound Iron Porphyrin Complex: Electrostatic versus Covalent Contribution to Bonding

Pradip Kumar Das and Abhishek Dey*

Department of Inorganic Chemistry, Indian Association for the Cultivation of Science, Kolkata, India 700032

Supporting Information

ABSTRACT: Resonance Raman (rR), electron paramagnetic resonance (EPR), and density functional theory (DFT) calculations of a phenolate-bound iron porphyrin complex are reported. The complex is found to exist in a five-coordinate high-spin state in a noncoordinating solvent and in a six-coordinate low-spin state in a coordinating solvent. The vibrations originating from the iron phenolate-bound chromophores reproduced those reported for heme tyrosine active sites in nature. The EPR parameters and iron−pyrrole ($Fe-N_{pyr}$) vibrations of phenolate, thiolate, and imidazole ligated iron porphyrin complexes indicate that the phenolate axial ligand acts as a π anisotropic ligand, which is more covalent than a neutral imidazole ligand but less covalent than a thiolate axial ligand. While the $Fe^{III/II}$ potential of the phenolate compound in a noncoordinating solvent is 500 mV more negative than that of the imidazole-bound complex, it is also 110 mV more negative than that of the thiolate-bound complex. DFT calculations reproduce the geometry and vibrational frequencies and show that while both phenolate and thiolate axial ligands bear π and σ interaction with the ferric center, the former is significantly less covalent than the thiolate. The higher covalency of the thiolate ligand is responsible for the lower $Fe-N_{pyr}$ vibration and higher V/λ (from EPR) of the thiolate-bound complexes relative to those of the phenolate-bound complex, whereas the greater electrostatic stabilization of the $Fe^{III}-OPh$ bond is responsible for lowering the $Fe^{III/II}$ $E°$ of the phenolate-bound complex relative to that of the thiolate-bound complex in a medium having a reasonable dielectric constant.

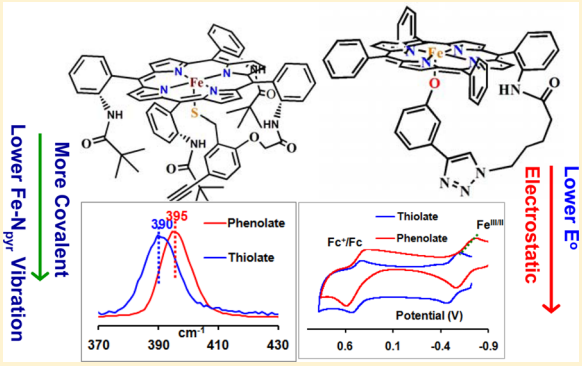

INTRODUCTION

The ability of axial ligands to modulate the chemistry of iron porphyrins has been an area of considerable interest for many years.[1−5] Most of the chemistry has been, however, focused on thiolate- and imidazole-bound iron porphyrin complexes because of the ubiquity of heme-containing proteins bearing a cysteine (which bears a thiolate side chain) and histidine (which bears an imidazole side chain) axial ligands.[3,6−12] In the case of heme catalases and some variants of hemoglobin, the heme cofactor is bound to phenolate oxygen from a tyrosine residue (Figure 1).[13−15] The sixth coordination is less clear, and a water molecule is often proposed to be ligated in the resting form. It appears to be vacant in the resting bovine liver catalase, as judged from the absence of electron density above the iron in the X-ray diffraction data, whereas electron density near the distal histidine in *Penicillium vitale* catalase might be due to a water molecule.[15−17] This enzyme is highly efficient at catalyzing the dismutation of hydrogen peroxide and is only able to oxidize low molecular weight alcohols (e.g., methanol, ethanol) using H_2O_2.[18−20] Catalase has one of the highest turnover numbers of all known metalloenzymes; one catalase molecule can convert millions of molecules of hydrogen peroxide to water and oxygen every second.[21] In the course of the enzymatic cycle, the active site of catalase gets oxidized to

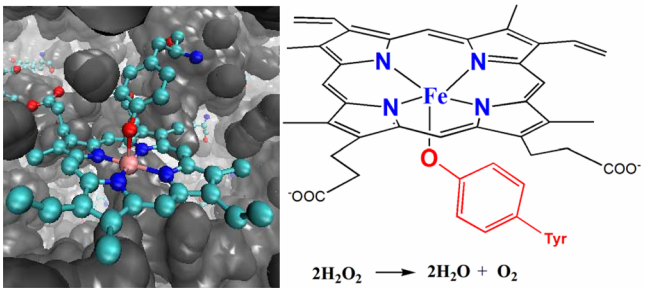

Figure 1. (Left) Active site structure of bovine liver catalase enzyme (pdb id: 8CAT). (Right) Chemical representation of the active site of catalase and the reaction it catalyzes.

produce a highly reactive species known as compound 1.[1,15,22−25] This species is best described as a high valent $Fe^{IV}=O$ species with a radical cation localized on the porphyrin ring.[20,22,26−30] Similar species have been generated in other heme proteins like cytochrome P450[11,31−38] and even in O_2 carrier proteins like hemoglobin (Hb)[39,40] and myoglobin

Received: March 27, 2014
Published: July 2, 2014

   dx.doi.org/10.1021/ic500716d | *Inorg. Chem.* 2014, 53, 7361−7370

(Mb).[41−43] The Fe center in the active site of the catalase in its resting form is best described as a five-coordinate (5C) high-spin (HS) Fe^{III}. Catalases are difficult to reduce under physiological conditions, as their $Fe^{III/II}$ $E°$ values are quite low (<500 mV) in solution and can be stabilized only via the formation of a CO adduct after photochemical reduction.[44,45] This is a very important attribute of the catalase active site as the reaction of H_2O_2 with a ferrous center will lead to Fenton type reaction and generate reactive oxygen species.

Heme bound to tyrosine ligands was known previously only in hemoglobin (Hb) mutants.[46,47] The crystal structure of Hb M Boston shows that the distal histidine is replaced by a tyrosine that coordinates to the Fe^{III} and displaces the usual proximal His, yielding a five-coordinated iron that is incapable of O_2 binding.[47] In Hb M Iwate, the proximal histidine is replaced by tyrosine; low resolution X-ray data indicate that the iron is hexacoordinated, binding both the abnormal tyrosine and the distal His.[46] Resonance Raman (rR) spectra of these mutant hemoglobin proteins were investigated by Nagai et al., and these data revealed several vibrational bands between 1300 and 1320 cm^{-1} characteristic of a tyrosinate coordination.[47,48] So far, few synthetic models of the catalase active site that mimic the axial phenolate coordination to a Fe^{III} porphyrin have been reported.[14,28,30,49,50] In these complexes, where an external phenolate ligand was used to bind Fe^{III} porphyrins, the effects of hydrogen bonding interactions on the redox properties of these complexes were investigated.[49]

Recently, a series of iron porphyrin complexes with axial imidazole, thiolate, and phenolate ligands were reported.[7,28,51] These ligands, which are tethered to the porphyrin macrocycle, stay bound to the metal ion in both oxidized and reduced forms.[52] The anionic thiolate ligand lowered the $Fe^{III/II}$ $E°$ by 400 mV relative to that with a neutral imidazole ligand.[7] Relative to a neutral imidazole ligand, anionic phenolate and thiolate ligands increased the rate of electrocatalytic oxygen reduction (ORR) in an aqueous medium by 10 and 100 times, respectively,.[51] The iron−pyrrole ($Fe-N_{pyr}$) vibration varies between 370 and 405 cm^{-1} and is found to be sensitive to the oxidation and spin state of the iron and even to the extent of covalent donation of the axial ligand.[53−55] It was observed at 400 cm^{-1} for a neutral imidazole ligand and at 390 cm^{-1} for an anionic thiolate ligand.[7] After comparing the Fe−O vibrations of an $Fe-O_2$ adduct, we suggested that the "push" effect of the tholate ligand is greater than that of the phenolate ligand which, in turn, is greater than that of the imidazole ligand.[52] Previous investigations using spectroscopic and computational techniques have suggested that Fe−O bonding has a greater electrostatic contribution than Fe−S bonding.[56,57] How these differences in bonding affect the electronic structure and spectroscopic properties of thiolate and phenolate-bound iron porphyrin complexes remains to be explored.

In this study, the spectroscopic (electron paramagnetic resonance (EPR), rR) and redox properties of a phenolate-bound iron porphyrin complex (POR, Figure 2) are compared to those of heme catalases and analogous thiolate-bound (PPSR-yne, Figure 2) and imidazole-bound (PIM, Figure 2) complexes. The results suggested that while there are certain similarities between the ground state (GS) wave functions of thiolate- and phenolate-bound iron porphyrin complexes, differences in the extent of electrostatic and covalent interaction between the two lead to distinct spectroscopic and redox properties.

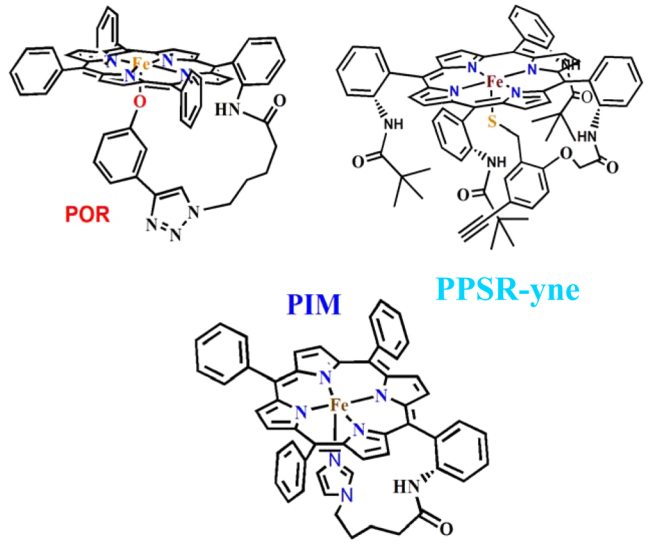

Figure 2. Schematic representation of the complexes.

EXPERIMENTAL SECTION

The complexes were synthesized using a reported procedure.[7,51,52]

Instrumentation. The EPR spectra were recorded on a JEOL instrument. All electrochemical experiments were performed using a CH Instruments Electrochemical Analyzer (model CHI710D). Resonance Raman (rR) data were collected using a 413.1 nm excitation wavelength from a Kr^+ ion source (Coherent, Sabre Innova SBRC-DBW-K) and a Trivista 555 triple spectrophotometer (gratings used in the three stages were 900, 900, and 1800 grooves/mm) fitted with a Pixis CCD camera (Princeton Instruments). The optics (e.g., plano−convex lenses, mirrors, etc.) for the collection of rR data were purchased from Sigma Koki.

Electrochemical Measurements. The CV was performed on CH instruments. A glassy carbon electrode was used as a working electrode. A Pt wire was used as a counter electrode. The measurements were made against a Ag/AgCl reference electrode with scan rates varying from 50 to 500 mV. The concentration of the prepared solution was 1 mM, and 100 mM tetrabutylammoniumperchlorate was used as the electrolyte.

Computational Method. All calculations are performed on the IACS Inorganic Chemistry HPC using Gaussian 03 version C02.[58] The geometries were optimized using BP86 and B3LYP functionals using the 6-311g* basis set on Fe, O, and N atoms and the 6-31g* basis set on C and H atoms.[59,60] Frequency calculations were performed using the same basis set, and no negative frequencies were found. The single-point calculations used the 6-311+g* basis set on all atoms. The orbital compositions were determined using the QMForge program, and Mulliken population analysis,[61] as implemented in the G03 code, was used to determine the charge and spin densities. For the calculation of reduction potential, the value of a free electron was assumed to be 4.43 eV, and a PCM model with dichloromethane (DCM) solvent is used.[62,63]

RESULTS

1. Absorption Spectroscopy. The absorption spectrum of POR complex shows a Soret band at 418 nm and several weaker Q bands at 518, 569, and 638 nm (deep green and inset in Figure S1, Supporting Information). These bands are distinct from those of the precursor POHR complex and that of the free ligand (violet and pink, Figure S1, Supporting Information). The POHR complex has several absorption bands in the visible region at 510, 578, and 688 nm which shift to 518, 569, and 638 nm, respectively, in the phenolate-bound Fe^{III} complex (POR) (Figure S1, Supporting Information).

dx.doi.org/10.1021/ic500716d | Inorg. Chem. 2014, 53, 7361−7370

2. Electron Paramagnetic Resonance (EPR). The X-band EPR data of the POR complex in weakly coordinating solvents like THF show an axial high-spin (HS) signal at $g = 6$ (Figure 3, green), indicative of an $S = 5/2$ GS. This is

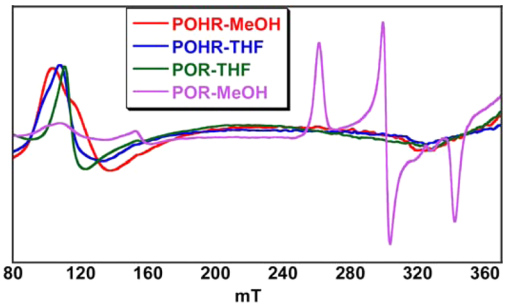

Figure 3. X-band EPR data of the POR and POHR complexes in THF and MeOH at 77 K, 10 mW power, and 1×10^4 gain.

consistent with the $S = 5/2$ GS observed in the active site of catalases.[13,16] The EPR data of the precursor phenol POHR complex also show an HS signal under the same condition. In a coordinating solvent like MeOH, POHR shows an $S = 5/2$ axial EPR signal with slight rhombic distortion (g = 6.2, 5.8), suggesting formation of a MeOH-bound complex (POHR–MeOH) but retaining its HS GS (Figure 3, red). On the contrary, the phenolate-bound iron POR complex shows an $S = 1/2$ GS with g values at 2.49, 2.16, and 1.89 at 77 K in a coordinating solvent like MeOH (Figure 3, violet). Thus, POR forms $S = 5/2$ species in weakly coordinating solvent like THF and $S = 1/2$ species in a coordinating solvent like MeOH. The rhombic parameter (V/λ) of the LS $S = 1/2$ signal, calculated using the Taylor analysis,[64] is consistent with the values obtained for LS analogues of the catalase active site and indicates the presence of a strong π anisotropic ligand like phenolate (Table 1).[65] Note the V/λ for the thiolate-bound LS

Table 1. EPR Parameters for the Heme Complexes

	spin	g_1	g_2	g_3	V/λ
catalase resting[66]	5/2	6.0			
catalase-N_3^-[66,67]	1/2	2.50	2.26	1.87	3.98
cyt P450[65]	1/2	2.45	2.26	1.91	4.59
POR	5/2	6.0			
POR–MeOH	1/2	2.49	2.16	1.89	4.02
PPSR-yne–MeOH	1/2	2.33	2.21	1.91	5.68

PPSR-yne complex is 5.68, which is much greater than that of the POR–MeOH complex. This is later addressed using density functional theory (DFT) calculations (vide infra).

3. Resonance Raman (rR). Resonance Raman spectra of the POR complex are obtained at 77 K with 413.1 nm excitation (Figure 4). The POR complex in THF shows that the oxidation and spin state marker ν_4 and ν_2 bands are at 1364 and 1555 cm^{-1}, respectively (Figure 4, pink). These values indicate that Fe center in the POR complex in THF is HS Fe(III),[68] consistent with the EPR data. Note that there is some reduced HS Fe(II) component in the spectrum with ν_4 and ν_2 vibrations at 1347 and 1535 cm^{-1}, respectively.[68] This is due to photoreduction of POR in the laser (Figure S2, Supporting Information). The rR data of the precursor POHR complex in THF show that the ν_4 and ν_2 bands are at 1363 and 1552 cm^{-1} (Figure S3, Supporting Information), respectively. However,

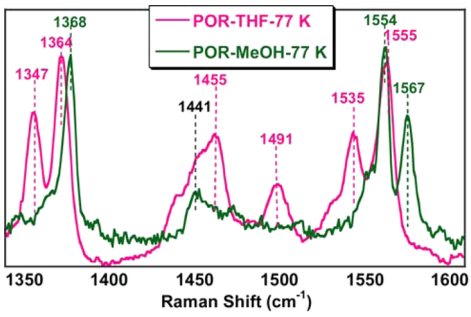

Figure 4. rR data in the high-energy region (1300–1600 cm^{-1}). Laser excitation wavelength = 413.1 nm; power = 10 mW.

the rR spectrum of the POR in MeOH (Figure 4, deep green) shows that the ν_4 and ν_2 bands are at 1368 and 1567 cm^{-1}, respectively, indicating that it exists as a six-coordinated LS species, consistent with the EPR data.[68] The rR data, along with the EPR data, indicate that the Fe center in the POR and POHR complexes in THF are HS Fe^{III}, and while the Fe center in the POHR complex retains its HS ground state in MeOH, the POR complex in MeOH exists in a LS state.

Proteins and synthetic model complexes bearing iron phenolate bonds (or iron tyrosinate in a protein active site) exhibit highly characteristic resonance-enhanced vibrational modes of the coordinated phenolate ligand.[13,69] In general, the Fe^{III}–O vibration of Fe^{III}–phenolate species lies between 530 and 600 cm^{-1} (Table 2).[15] The rR spectra, in the low-frequency

Table 2. Characteristic Resonance Raman Frequencies (cm^{-1}) for Fe(III)–Phenolates Complexes

active site	ν(Fe–O)	ν(C–O)	ref
hemoglobin M Boston	603	1279	48
hemoglobin M Iwate	588	1308	70
bovine liver catalase		1244 (?)	15
$[Fe(TTOP)]_2$	623	1293	15
POR	573, 589	1320	this work

region of the POR complex , show peaks at 573 and 589 cm^{-1} corresponding to Fe–OPh vibrations (Fe–O stretch and ν_{6b}) (Figure 5A, blue), consistent with the values reported for the active site of tyrosine-bound heme sites (Table 2).[69,70] These vibrations are not observed for the precursor POHR complex (which bears a protonated phenol), the reduced POR complex, and PIM and PPSR-yne complexes (Figures 5A and 6). This supports the assignments of these vibrations as the Fe^{III}–O stretch resulting from the phenolate coordination to Fe^{III}–porphyrin. Note that two Fe–O vibrations are observed instead of one. This is analyzed using DFT calculations. Multiple features are observed between 1100 and 1600 cm^{-1}, which is typical of metal phenolate complexes and consistent with the values reported for the catalase enzyme (Figure S4, Supporting Information) and other Fe^{III}–phenolate complexes.[15] Unfortunately, many of these vibrations overlap with the porphyrin ring modes.[71] However, the C–O stretch at 1320 cm^{-1} is clearly observed in the POR complex and not in the POHR, PIM, and PPSR-yne complexes, further supporting phenolate coordination in the POR complex (Figure 5B; Figure S5, Supporting Information). A vibration in the range of 1280–1320 cm^{-1} is generally associated with a heme tyrosine active site (Table 2).[48] Note that while the vibrations observed for POR are consistent with those observed for mutants of Hb bearing an

dx.doi.org/10.1021/ic500716d | Inorg. Chem. 2014, 53, 7361–7370

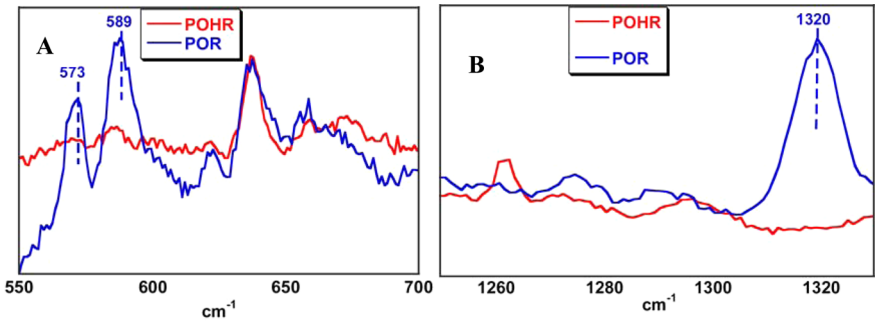

Figure 5. rR data in the low-energy region in THF at 77 K. Laser excitation wavelength = 413.1 nm; power = 10 mW.

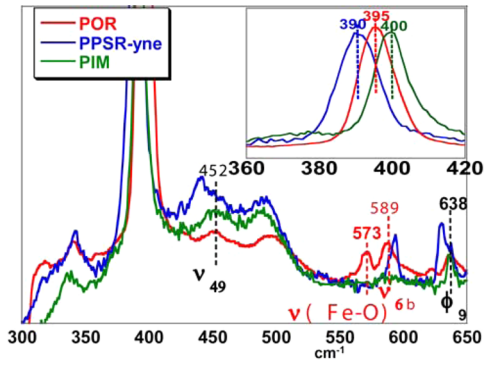

Figure 6. rR data in the low-energy region in THF at 77 K. Laser excitation wavelength = 413.1 nm; power = 10 mW.

axial tyrosine ligand and another synthetic model complex, these vibrations are not resolved for catalase active sites.[15,48,70] Generally, Fe−O vibrations have been selectively enhanced with excitation near 500 nm.[15,69] However, here, the rR data suggest that the Fe−O vibrations are observed by exciting into the Soret band. This implies mixing of the porphyrin and the Fe−OPh bonding orbitals in these complexes (vide infra).

The ν_8 vibration, which represents the Fe−N_{pyr} (iron−pyrrole nitrogen) symmetric stretch, is observed at 395 cm^{-1} for the S = 5/2 POR in THF (Figure 6, red).[71] The Fe−N_{pyr} vibration reflects the relative donor strengths of the axial ligands between complexes having the same spin states (Table 3). The

Table 3. ν_8 (Fe−N_{pyr} Stretch) Vibrations (cm^{-1}) of the Complexes

complex	THF	MeOH
POR	395	391
PPSR-yne	390	389
PIM	400	395

data suggest that the S = 5/2 PIM complex, which has an axial imidazole ligand, has an Fe−N_{pyr} vibration (400 cm^{-1}) higher than that of the S = 5/2 PPSR-yne and POR complexes, which have a thiolate and phenolate axial ligand, respectively. This indicates that the thiolate and phenolate axial ligands are much better donors than imidazole. Further, the Fe−N_{pyr} vibration of the thiolate-bound PPSR-yne is at 390 cm^{-1}, which is 5 cm^{-1} weaker than the Fe−N_{pyr} vibration of the phenolate-bound POR complex (395 cm^{-1}). Similarly, the Fe−N_{pyr} vibration of the LS PIM−MeOH, POR−MeOH, and PPSR-yne−MeOH complexes are at 395, 391, and 389 cm^{-1}, respectively, showing the same trend observed for the 5C HS complexes (Figure S6, Supporting Information). DFT calculations have been utilized to understand this effect in detail (vide infra).

4. Cyclic Voltammetry (CV). Cyclic voltammetry of the POR complex shows one oxidation reduction process (Figure 7, red). The quasi-reversible wave with an $E_{1/2}$ of −1.14 V

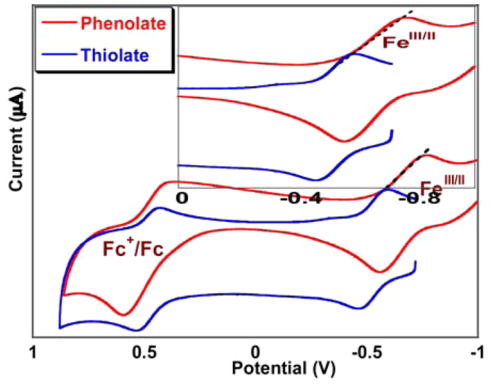

Figure 7. CV of the above complexes in a CH_2Cl_2 solvent having 100 mM TBAP as supporting electrolyte, glassy carbon as the working electrode, a scan rate of 100 mV/s, and Fc/Fc^+ as an internal reference electrode.

represents the $Fe^{III/II}$ couple, consistent with the values reported for other phenolate-bound iron porphyrin complexes.[49] The thiolate complex shows a reversible wave with an $E_{1/2}$ of −1.03 V representing the $Fe^{III/II}$ couple (Figure 7, blue). For an analogous imidazole ligated complex PIM, $E_{1/2}$ is −0.58 V, as reported previously.[7] Thus, the presence of the axial anionic π donor ligand lowers the $Fe^{III/II}$ potential by 560 mV relative to that of the neutral imidazole ligand. The reduction potential of the POR complex is thus 110 mV more negative than that of the thiolate complex. The lower $E°$ of the phenolate complex relative to the thiolate complex reproduces the lower $E°$ of the 5C HS catalase site relative to P450 in solution.[12,44,45,50] Note that based on the relative magnitude of the Fe−N_{pyr} vibration with an axial thiolate ligand and having the lowest Fe−N_{pyr} vibration (i.e., the weakest Fe−N_{pyr} bond), this complex may have been expected to have the lowest $Fe^{III/II}$ $E°$ of the three. Contrary to expectations, the phenolate complex has an $Fe^{III/II}$ $E°$ that is 110 mV lower than that of the thiolate complex. This difference likely originates from an electrostatic interaction between Fe and O in phenolate that is stronger than that between Fe and S in thiolate and is analyzed using DFT calculations (vide infra).

5. DFT Calculations. *5.1. Geometry.* Geometry-optimized DFT calculations are performed to obtain a possible structure of the POR complex in its HS and LS forms (Figure 8).[58,59]

dx.doi.org/10.1021/ic500716d | Inorg. Chem. 2014, 53, 7361−7370

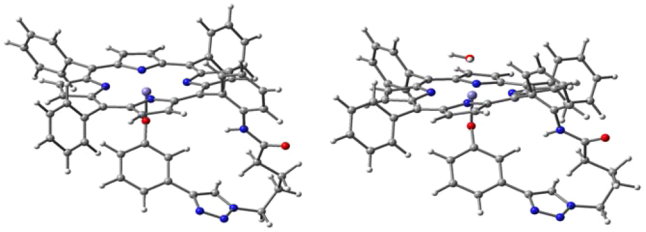

Figure 8. DFT-optimized structures of POR and POR–H_2O complexes.

The optimized geometries obtained using the BP86 functional indicate the Fe–O bonds are 1.84 and 1.81 Å in the 5C HS and the 6C LS states, respectively (Table 4; values obtained with B3LYP provided in Table S7, Supporting Information). These values are in good agreement with the reported structures of catalase active sites as well as those of synthetic model complexes.[49,50] The Fe–OH_2 bond, present in the 6C LS model, is 2.10 Å, which is in good agreement with previous reports on LS Fe^{III} complexes bearing a bound H_2O.[7] The Fe–N_{pyr} bonds are longer by 0.01 Å in the HS thiolate-bound PSR complex than that of the tyrosine-bound HS POR complex, indicating a weaker Fe–N_{pyr} bond in the former. Similarly, the Fe–N_{pyr} bonds of the HS imidazole-bound PIM complex are 2.05 Å, which is shorter than those in the PSR (a smaller model for PPSR-yne) and POR complexes, respectively.

The Fe–O–Ph angle in BLC (X-tal) and POR (optimized) is ∼140° in the high-spin state. The larger Fe–O–Ph angle in POR likely leads to kinematic coupling of the Fe–O and the ν_{6b} mode resulting in enhancement of both at the same time.

5.2. Vibrations. The calculated vibrational frequencies (using both BP86 and B3LYP) are listed in Table 5. The calculations using the BP86 functional reproduce the experimentally observed symmetric ν_4 and ν_2 intraligand modes for the phenolate-bound complex with good accuracy (within ±20 cm^{-1}, ∼1% error). These calculations further reproduce the experimentally observed relative magnitudes in the ν_8 vibrations (i.e., the Fe–N_{pyr} stretch) of the HS complexes (i.e., PIM > POR > PSR). Thus, the BP86 functional is suitable for calculating these sets of molecules and is used for further calculations. Note that B3LYP underestimates the intraligand modes in general and, in particular, for PIM.

The calculated Fe–O–C angle of the complex is 145°, which is much wider than the angle of 109° that may be expected for an sp^3 hybridized O center. As a consequence of this wide Fe–O–C angle (also observed in the crystal structure of BLC, 143°), the Fe–O vibration couples (calculated to be at 613 cm^{-1}) with the ν_{6b} bending mode of the phenolate (calculated to be at 590 cm^{-1}) were also observed. Note that the Fe–L vibrations are overestimated by 2.8% at this level of theory. Enhancement of both the Fe–O and ν_{6b} of phenolate in the rR spectra is also observed for a bovine liver catalase, which has an Fe–O–C angle of 143°. This may explain the observation of two vibrations (Fe–O at 573 cm^{-1} and phenolate ν_{6b} at 589 cm^{-1}) instead of one Fe–O vibration in this region.

5.3. Electronic Structure. 5.3.1. 5C. The GS wave function of the HS 5C complex (POR) shows a $t_2^3e^2$ configuration with a square pyramidal ligand field. The $d_{x^2-y^2}$ orbital is highest in energy due to its σ antibonding interaction with the in-plane pyrrole orbitals. There are two interactions between the Fe and the phenolate ligand: a σ interaction between the out-of-plane phenolate π^* orbital and the d_{z^2} orbital (Figure 9, middle) and a π interaction between the in-plane phenolate π^* orbital and the d_{yz} orbital (Figure S4, Supporting Information). The interactions between the phenolate and the Fe are similar to those in other well-studied analogues; for alkyl thiolate, there are certain nuances worth mentioning. Note that the $d_{x^2-y^2}$ orbitals of the PIM complex are at higher energies than those of the POR and PSR complexes. The higher Z_{eff} on the Fe in the POR complex will result in stronger σ bonding and π interaction with the occupied anionic porphyrin donor ligand orbitals (in-plane pyrrole orbitals, in-plane phenolate π^* orbitals). This reflects the stronger Fe–N_{pyr} bonds in the POR complex relative to the PSR complex. The molecular orbital (MO) contributions in Table 6 reveal that the d_{yz} and d_{xz} orbitals in the POR model have 15% S_{3p} mixed into them, while the d_{z^2} orbital has 4% S_{3p} mixed into it; that is, there is significant covalent interaction between Fe and O (both σ and π). The t_2 orbitals contain contributions from both the phenolate ligand and the porphyrin. Similarly, the porphyrin π^* shows significant mixing of the phenolate ligand. This mixing between these two centers may provide a mechanism for how the Fe–O and C–O modes of POR are observed in the rR data when the Soret band ($\pi \rightarrow \pi^*$) is excited.

Notably, the spin density on the thiolate sulfur is significantly greater than that of the phenolate ligand in the HS state. This implies that, in spite of the Fe–S bond being significantly longer than the Fe–O bond, the Fe–S bond is much more covalent than the Fe–O bond. The lower charge transfer from the phenolate to Fe holds true for both the π and σ interactions.

Table 4. Optimized Bond Lengths (Å) and Angles (deg) of the Models and Relevant Mulliken Charges

		geometry					Mulliken charges	
		Fe–N_{pyr}	Fe–L[a]	C–O	Fe–O–C	Fe–X_{axial}	q_{Fe}	$q_{O/S/N}$
S = 5/2	***BLC***[b]	***2.02***	***1.89***	***1.39***	***142.8***			
	POR	2.08	1.84	1.33	145		1.54	−0.68
	PSR	2.09	2.31				1.41	−0.41
	PIM	2.05	2.08				1.52	−0.58
S = 2	POR	2.09	1.9	1.32	132.8		1.42	−0.69
	PSR	2.08	2.36				1.32	−0.55
S = 1/2	***BLC***[c]	***1.95***	***1.88***	***1.38***	***131***	***2.11***		
	POR	2.00	1.81	1.35	128	2.10	1.26	−0.58
	PSR	1.98	2.18			2.16	1.20	−0.33

[a]L = axial ligand coordinating atom; S for PPSR-yne, N for PIM, and O for POR. [b]Resting bovine liver catalase (8CAT). [c]N_3^--bound bovine liver catalse (1TH2).

dx.doi.org/10.1021/ic500716d | Inorg. Chem. 2014, 53, 7361–7370

Table 5. Calculated Vibrational Frequencies (cm^{-1})

	PSR[7]			POR			PIM		
mode	rR	BP86	B3LYP[a]	rR	BP86	B3LYP[a]	rR	BP86	B3LYP[a]
ν_2	**1554**	1551	1477	**1555**	*1550*	1525	**1551**	*1533*	*1482*
ν_3	**1451**	1447	1421	**1455**	*1458*	1432	**1461**	*1427*	*1420*
ν_4	**1361**	1351	1326	**1364**	*1351*	1325	**1361**	*1353*	*1308*
ν_8	**391**	378	373	**395**	*382*	378	**400**	*384*	*366*
C−O				**1320**	*1286*	1251			
Fe−S	**336**	308	290						
	369	369	303						
		410	351						
Fe−O				**573**	*590*	574			
				589	*614*	600			

[a]Values obtained using B3LYP are scaled by 0.95.[72]

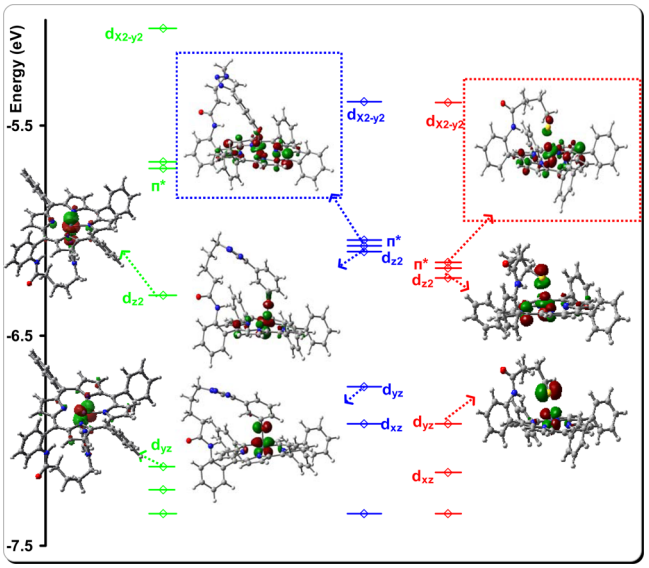

Figure 9. Calculated (BP86) GS MO diagram of 5C PIM, POR, and PSR complexes. Only unoccupied β orbitals are shown.

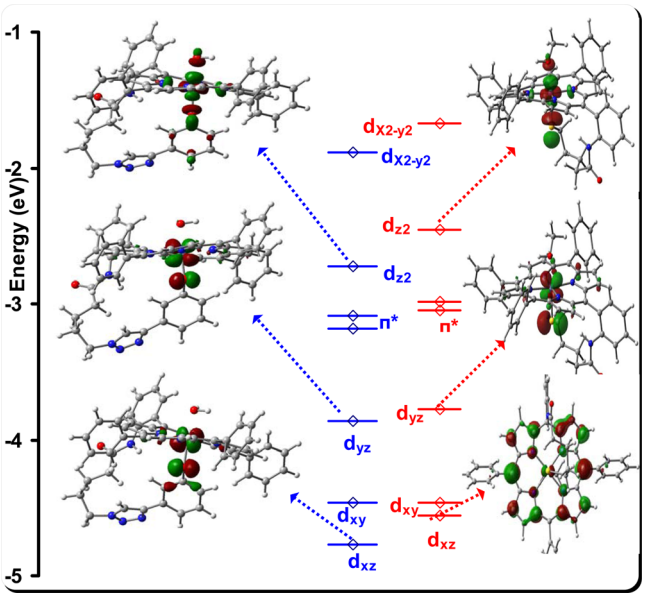

Figure 10. MO diagram of the 6C (left) POR−H_2O and (right) PSR−MeOH complexes.

5.3.2. 6C. The GS wave function of the LS 6C POR−H_2O complex is very similar to that of the PSR−MeOH complex. It has a distorted octahedral ligand field. The GS wave function of the 6C LS POR−H_2O complex shows a normal $t_2^5e^0$ electronic structure. The singly occupied t_2 orbital forms a π bond, while the unoccupied e orbital forms a σ bond with the in-plane and out-of-plane orbital of the phenolate ligand, respectively (Figure 10). In the POR−H_2O complex, ∼6% of occupied Fe t_2 character is mixed into the porphyrin π^* orbital, while for the PSR−MeOH complex, ∼8.2% of occupied Fe t_2 character is mixed into the porphyrin π^* orbital. This is due to higher energies of the Fe_{3d} orbital of the PSR−MeOH complex relative to the POR−H_2O complex as greater covalent charge donation from the anionic thiolate ligand to the iron in the PSR−MeOH complex (28% π + 2 × 26% σ = 0.8 e) lowers the Z_{eff} on the Fe and increases the energy of the 3d manifold. This allows better overlap with the t_2 orbitals and π^* orbital. Note that the d_{yz} orbital, the energy of which is increased by strong π bonding interaction with the thiolate, carries the unpaired electron.

Table 6. MO Compositions of the β Unoccupied Orbital

	orbital contribution								
	POR			PSR			PIM		
orbitals	Fe_{3d}	$O_{2p,2s}$	N_{pyr}	Fe_{3d}	S_{3p}	N_{pyr}	Fe_{3d}	$N_{2p,2s}$	N_{pyr}
$d_{x^2-y^2}$	67.08	0.01	15.42	68.01	0.00	14.92	66.51	0.00	16.49
π^*	19.56	**1.29**	7.16	22.74	**6.51**	7.17			
d_{z^2}	55.06	**3.66**	5.19	45.34	**15.87**	5.84	66.6	**6.69**	6.19
d_{yz}	61.81	**9.19**	1.89	53.48	**28.64**	1.8	72.1	0.91	2.89
d_{xz}	64.44	**5.55**	1.84	70.54	1.03	1.52	71.22	**2.29**	3.1
d_{xy}	90.44	0.04	0.43	89.47	0.42	0.42	85.49	0.08	1.32

dx.doi.org/10.1021/ic500716d | Inorg. Chem. 2014, 53, 7361−7370

Thus, while both the phenolate and the thiolate ligands exhibit considerable π and σ interaction with the $d_{yz/xz}$ and d_{z^2} orbitals (Table 7), the delocalization is significantly greater for the thiolate ligand; that is, the Fe−S bond is considerably more covalent that the Fe−OPh bond.

Table 7. Calculated Orbital Populations

complex	spin	π (d_{yz})	σ (d_{z^2})	total
PIM−MeOH	S = X	0.3	7.7	8 ($\pi + \sigma$)
	S = 1/2	0.2	10	20.2 ($\pi + 2\sigma$)
PSR−MeOH	S = 5/2	28	16	44 ($\pi + \sigma$)
	S = 1/2	28	26	80 ($\pi + 2\sigma$)
POR−H_2O	S = 5/2	10	4	14 ($\pi + \sigma$)
	S = 1/2	11	10	31 ($\pi + 2\sigma$)

5.4. Reduction Potential. DFT calculations were also used to calculate the $E°$ of these complexes. The calculated values cannot be directly compared to the experimental value, as these use different reference points; however, the relative magnitudes can be compared. The PSR complex is calculated to have an $E_{1/2}$ that is 34 mV more negative than that of the POR complex in the gas phase (Table 8). But when solvation is included (DCM), the POR complex is calculated to have a potential (7 mV) more negative than that of the PSR complex, reproducing the experimentally observed trend. This likely reflects differences in the nature of bonding in the PSR and POR complexes (vide infra).

Table 8. DFT Calculated Reduction Potentials in Volts (V)

complex	potential (gas phase)	potential (DCM)
PSR	−1.917	−0.784
POR	−1.883	−0.791

The dependence of $E°$ on Fe−L bond energy (BE) can be approximately expressed as

$$E° = BE_{ox} - BE_{red}$$

BE, on the other hand, can have both covalent and electrostatic contributions, that is,

$$BE = BE_{cov} + BE_{elec}$$

As indicated by the calculated GS wave function for the 5C HS state, the Fe−S bond has more covalent character than the Fe−OPh bond. The contribution of BE_{elec} can be approximately estimated by Coulomb's law;

$$BE_{elec} = Z_{eff}^{Fe} Z_{eff}^{L} / r_{Fe-L} \times 14.1 \text{ kcal/mol}$$

The calculated Mulliken charges on the Fe and S atoms for PSR and the Fe and O atoms for POR in the gas phase and after solvation are listed in Table 9.

The electrostatic interaction between the iron and the coordinating atom of the axial ligand is considered. For PSR, the electrostatic stabilization of the reduced state is greater than that of the oxidized state. On the contrary, the electrostatic stabilization of the oxidized state of POR is greater than that for the reduced state. This is a direct result of the strong covalent bonding between the thiolate sulfur and iron in the oxidized state, which reduces the partial charges on the individual centers, thus reducing the electrostatic contribution to bonding. The electrostatic contribution to bonding stabilizes the oxidized state of POR by 0.79 kcal/mol and destabilizes the oxidized state of the PSR complex by 0.74 kcal/mol. Thus, the electrostatic contribution favors the oxidation of the POR complex by 1.53 kcal/mol relative to the PSR complex. This may be expected to lower the reduction potential of the POR complex relative to that of the PSR complex by 66 mV. The corresponding calculated $E°$ of the PSR is 34 mV more negative in the gas phase. This, of course, represents the combined effect of the covalent and electrostatic contributions to bonding. In this case, the large covalency of the Fe−S bond in the oxidized state, as indicated in the reduction of the ν_8 vibration and the calculated GS wave function, results in an $E°$ for the PSR complex that is more negative than that of the POR complex.

The electrostatic stabilization increases when a PCM used as the polarization of the environment favors charge separation in the GS wave function. The enhanced electrostatic stabilization of the POR complex, on including solvation, in its oxidized form relative to the reduced form (0.94 kcal/mol) is now expected to lower its potential by 81 mV relative to the PSR complex, where the oxidized state is now destabilized by 0.92 kcal/mol. Thus, the inclusion of the polarized medium is expected to lower the $E°$ of the POR complex 80 mV (1.86 kcal/mol) relative to the PSR complex, 14 mV more relative to the gas phase. The calculated $E°$ for the PSR is 34 mV more negative in the gas phase, while the calculated $E°$ of POR is 7 mV more negative in DCM. Thus, the calculations show that inclusion of the PCM medium in the calculations shifts the POR $E°$ more negative by 41 mV relative to the PSR complex. This is likely due to the larger electrostatic stabilization of the oxidized POR complex.

DISCUSSION

The rR of the POR complex indicates that Fe−O and ν_{6b} vibrations of a 5C HS Fe−OPh unit are at 589 and 573 cm^{-1}, respectively. The C−O vibration of the phenolate ligand is identified at 1320 cm^{-1}. These values are consistent with those reported for the 5C HS resting state of heme proteins bearing a tyrosine axial ligand. The EPR and the oxidation/spin state

Table 9. Mulliken Charges and Electrostatic Interaction Energies

	Fe^{III}				Fe^{II}				
	q_{Fe}	q_x	r_{Fe-L}	E_{elec}	q_{Fe}	q_x	r_{Fe-L}	E_{elec}	ΔE_{elec}
	Gas Phase (ε = 1)								
PSR	1.45	−0.37	2.31	−3.27	1.37	−0.49	2.36	−4.01	+0.74
POR	1.59	−0.62	1.84	−7.55	1.47	−0.62	1.90	−6.76	−0.79
	in DCM Solution (ε = 8.9)								
PSR	1.46	−0.44	2.31	−3.92	1.38	−0.59	2.36	−4.86	+0.92
POR	1.60	−0.64	1.84	−7.84	1.46	−0.64	1.90	−6.90	−0.94

dx.doi.org/10.1021/ic500716d | Inorg. Chem. 2014, 53, 7361−7370

marker bands of the POR complex show that it becomes 6C LS in a coordinating solvent like MeOH. The g values are anisotropic, and the V/λ ratio, obtained from Taylor analysis, indicates that the phenolate ligand is a strong π anisotropic ligand.

The V/λ of the POR complex is 4.02, which is less than that of a corresponding axial thiolate ligand-bound complex PPSR-yne, which is 5.68. The ν_8 vibration, which is a reporter of the extent of charge donation from the axial ligand to the iron, of the POR complex is 395 cm^{-1}, which is less than that of an imidazole-bound complex, PIM, but higher than that of the thiolate-bound complex PPSR-yne (390 cm^{-1}). The higher ν_8 of PIM, relative to that of the POR complex, indicates that the axial phenolate is more covalent than the axial imidazole. Alternatively, both the V/λ and lower ν_8 indicate that the POR complex is less covalent than an axial thiolate ligand. This is substantiated by DFT calculations that reproduce the experimentally observed vibrational parameters (Table 5, in italics). The calculated wave functions show that the axial phenolate ligand has σ and π bonding interactions with the d_{z^2} and $d_{xz/yz}$ orbitals in both the 5C HS and 6C LS states. The 5C wave function shows 15 and 4% mixing of the phenolate ligand into the π bonding $d_{xz/yz}$ and σ bonding d_{z^2} orbitals, respectively. These are much lower than the 29 and 16% mixing of the thiolate ligand into the π and σ bonding d orbitals, respectively. Similarly, for the 6C LS GS, the π and σ antibonding d orbitals have 11 and 20% phenolate mixed into them, respectively. While the contributions of the phenolate ligand to the metal 3d wave functions increase significantly relative to those of the 5C HS state, these are still much lower than those of an axial thiolate ligand, which show 28 and 52% mixing into the π and σ 3d orbitals, respectively.

The lower charge donation from the phenolate oxygen to the Fe relative to the thiolate sulfur results in a larger contribution of electrostatic interaction to the Fe−L bond in the former and a more covalent contribution in the latter. This produces an interesting anomaly between measured properties. The measured vibrational and EPR data clearly indicate that the Fe−SR bond is more covalent than the Fe−OPh bond. On the contrary, the measured $E°$ of the POR complex is 110 mV more negative than that of the PPSR-yne complex in DCM. Normally, with other ligands remaining the same, a more covalent axial ligand would result in a lower $E°$. For example, the PIM complex with a neutral imidazole axial ligand has an $E°$ 400−500 mV more positive than that of PPSR-yne and POR. Thus, considering the higher covalency of the Fe−SR bond in the PPSR-yne complex, it may be expected to have an $E°$ lower than that of the POR complex. This is not the case. DFT calculations indicate that indeed, in the gas phase, the calculated $E°$ for the PSR complex is lower than that of the POR complex. However, calculations that include solvation show that the POR complex has an $E°$ lower than that of the PSR complex. This is due to the greater electrostatic contribution to axial ligand Fe bonding in the less covalent POR complex relative to the PSR complex, which has a very covalent Fe−S bond. The electrostatic interaction contributes more in a polarized medium relative to the gas phase. This leads to significant stabilization of the oxidized Fe^{III} state in the POR complex, which results in a decrease in its $Fe^{III/II}$ $E°$ relative to that of the PSR complex in DCM.

Of the three axial ligands prevalent in the heme active sites, phenolate and thiolate are both anionic. The additional negative charge in the P450 active site lowers the pK_a of trans ligands such that the compound II species is protonated (Fe^{IV}−OH), whereas compound II in neutral imidazole-bound sites is deprotonated (Fe^{IV}=O).[31,72,73] Additionally, the covalent donation from the anionic axial thiolate ligand helps stabilize high valent intermediates in the P450 type active sites, and the basicity of the Fe^{IV}=O unit in the oxidant, compound I, helps achieve strong C−H bond abstraction using a low-potential oxidant.[11,38,74−76,] Catalases, on the other hand, are bound via an anionic ligand, giving it a distinct edge over neutral imidazole-bound active sites in stabilizing high valent species that are characterized by a lower Fe^{III}/Fe^{II} $E°$ (−226 on electrode to <500 mV in solution) relative to P450 (−175 mV in solution) in their 5C HS resting form.[44,45,77,78]

The results presented in this study suggest that differences in covalent and electrostatic contributions to the ground state electronic structures of these anionic phenolate- and thiolate-bound heme active sites play a major role in determining their biophysical properties. The thiolate axial ligand forms more covalent Fe−S bonds, which lowers the Lewis acidity of the iron center, whereas the phenolate axial ligand forms less covalent bond and results in higher Lewis acidity at the metal site. As a result, the water-derived axial ligands at the P450 active site will have pK_a values greater than that of the catalase active site. The fact that compound II is protonated in P450 but deprotonated in compound II in catalase serves as an illustrative example.[77,79]

The lower $E°$ of a phenolate-bound iron porphyrin complex relative to that of a thiolate- or imidazole-bound complex suggests yet another role the tyrosine axial ligand may be playing in the active site of catalase. Presumably, it is absolutely essential to avoid the reduction of the heme site of catalase to its ferrous state under physiological conditions as reaction of H_2O_2, its substrate, with the reduced ferrous site will result in the generation of reactive oxygen species by Fenton's reaction. The results obtained using POR suggest that the enhanced stabilization of the oxidized state in a medium with low dielectric (organic solvent for POR and protein environment for catalase) resulting from the electrostatic nature of the Fe−O bond is likely to be responsible for the very low $Fe^{III/II}$ potential observed in the catalase active site, preventing its reduction by most physiological reducing agents.

■ ASSOCIATED CONTENT

Supporting Information

rR data of phenol complexes, optimized geometries, and full ref 58. This material is available free of charge via the Internet at http://pubs.acs.org.

■ AUTHOR INFORMATION

Corresponding Author

*E-mail: icad@iacs.res.in.

Notes

The authors declare no competing financial interest.

■ ACKNOWLEDGMENTS

This work is funded by the Council of Scientific and Industrial Research (CSIR), India [Grant 01(2412)10/EMr-II], and the Department of Science and Technology, India (Grant SR/IC-35/2009). P.K.D. acknowledges a CSIR SRF fellowship.

■ REFERENCES

(1) Dawson, J. H. *Science* **1988**, *240*, 433−439.

(2) de Visser, S. P.; Latifi, R.; Tahsini, L.; Nam, W.-W. *Chem.—Asian J.* **2011**, *6*, 493−504.
(3) Green, M. T. *J. Am. Chem. Soc.* **1998**, *120*, 10772−10773.
(4) Poulos, T. L. *Nat. Struct. Mol. Biol.* **1996**, *3*, 401−403.
(5) Wuttke, D. S.; Gray, H. B. *Curr. Opin. Struct. Biol.* **1993**, *3*, 555−563.
(6) Collman, J. P.; Gagne, R. R.; Reed, C.; Halbert, T. R.; Lang, G.; Robinson, W. T. *J. Am. Chem. Soc.* **1975**, *97*, 1427−1439.
(7) Das, P. K.; Chatterjee, S.; Samanta, S.; Dey, A. *Inorg. Chem.* **2012**, *51*, 10704−10714.
(8) Meunier, B.; de Visser, S. P.; Shaik, S. *Chem. Rev.* **2004**, *104*, 3947−3980.
(9) Ogliaro, F.; Cohen, S.; de Visser, S. P.; Shaik, S. *J. Am. Chem. Soc.* **2000**, *122*, 12892−12893.
(10) Paulat, F.; Lehnert, N. *Inorg. Chem.* **2007**, *46*, 1547−1549.
(11) Rittle, J.; Green, M. T. *Science* **2010**, *330*, 933−937.
(12) Suzuki, N.; Higuchi, T.; Urano, Y.; Kikuchi, K.; Uekusa, H.; Ohashi, Y.; Uchida, T.; Kitagawa, T.; Nagano, T. *J. Am. Chem. Soc.* **1999**, *121*, 11571−11572.
(13) Que, L., Jr. *Coord. Chem. Rev.* **1983**, *50*, 73−108.
(14) Robert, A.; Loock, B.; Momenteau, M.; Meunier, B. *Inorg. Chem.* **1991**, *30*, 706−711.
(15) Sharma, K. D.; Andersson, L. A.; Loehr, T. M.; Terner, J.; Goff, H. M. *J. Biol. Chem.* **1989**, *264*, 12772−12779.
(16) Fita, I.; Rossmann, M. G. *J. Mol. Biol.* **1985**, *185*, 21−37.
(17) Vainshtein, B. K.; Melik-Adamyan, W. R.; Barynin, V. V.; Vagin, A. A.; Grebenko, A. I.; Borisov, V. V.; Bartels, K. S.; Fita, I.; Rossmann, M. G. *J. Mol. Biol.* **1986**, *188*, 49−61.
(18) Belal, R.; Momenteau, M.; Meunier, B. *J. Chem. Soc., Chem. Commun.* **1989**, 412−414.
(19) Corrall, R. J. M.; Rodman, H. M.; Margolis, J.; Landau, B. R. *J. Biol. Chem.* **1974**, *249*, 3181−3182.
(20) Dunford, H. B.; Stillman, J. S. *Coord. Chem. Rev.* **1976**, *19*, 187−251.
(21) Nicholls, P.; Fita, I.; Loewen, P. C. *Adv. Inorg. Chem.* **2000**, *51*, 51−106.
(22) Chuang, W. J.; Van Wart, H. E. *J. Biol. Chem.* **1992**, *267*, 13293−13301.
(23) Kincaid, J. R.; Zheng, Y.; Al-Mustafa, J.; Czarnecki, K. *J. Biol. Chem.* **1996**, *271*, 28805−28811.
(24) Paeng, K. J.; Kincaid, J. R. *J. Am. Chem. Soc.* **1988**, *110*, 7913−7915.
(25) Regelsberger, G.; Jakopitsch, C.; Engleder, M.; Rüker, F.; Peschek, G. n. A.; Obinger, C. *Biochemistry* **1999**, *38*, 10480−10488.
(26) Czarnecki, K.; Kincaid, J. R.; Fujii, H. *J. Am. Chem. Soc.* **1999**, *121*, 7953−7954.
(27) Dolphin, D.; Forman, A.; Borg, D. C.; Fajer, J.; Felton, R. H. *Proc. Natl. Acad. Sci. U.S.A.* **1971**, *68*, 614−618.
(28) Fujii, H.; Yoshimura, T.; Kamada, H. *Inorg. Chem.* **1997**, *36*, 6142−6143.
(29) Hager, L. P.; Doubek, D. L.; Silverstein, R. M.; Hargis, J. H.; Martin, J. C. *J. Am. Chem. Soc.* **1972**, *94*, 4364−4366.
(30) Takahashi, A.; Kurahashi, T.; Fujii, H. *Inorg. Chem.* **2009**, *48*, 2614−2625.
(31) Dawson, J. H.; Sono, M. *Chem. Rev.* **1987**, *87*, 1255−1276.
(32) Green, M. T. *J. Am. Chem. Soc.* **1999**, *121*, 7939−7940.
(33) Newcomb, M.; Zhang, R.; Chandrasena, R. E. P.; Halgrimson, J. A.; Horner, J. H.; Makris, T. M.; Sligar, S. G. *J. Am. Chem. Soc.* **2006**, *128*, 4580−4581.
(34) Rittle, J.; Younker, J. M.; Green, M. T. *Inorg. Chem.* **2010**, *49*, 3610−3617.
(35) Schöneboom, J. C.; Neese, F.; Thiel, W. *J. Am. Chem. Soc.* **2005**, *127*, 5840−5853.
(36) Schlichting, I.; Berendzen, J.; Chu, K.; Stock, A. M.; Maves, S. A.; Benson, D. E.; Sweet, R. M.; Ringe, D.; Petsko, G. A.; Sligar, S. G. *Science* **2000**, *287*, 1615−1622.
(37) Shaik, S.; Kumar, D.; de Visser, S. l. P.; Altun, A.; Thiel, W. *Chem. Rev.* **2005**, *105*, 2279−2328.
(38) Sligar, S. G. *Science* **2010**, *330*, 924−925.
(39) De Jesús-Bonilla, W.; Cortés-Figueroa, J. E.; Souto-Bachiller, F. A.; Rodríguez, L.; López-Garriga, J. *Arch. Biochem. Biophys.* **2001**, *390*, 304−308.
(40) Roman, R.; Dunford, H. B. *Biochemistry* **1972**, *11*, 2076−2082.
(41) Egawa, T.; Shimada, H.; Ishimura, Y. *J. Biol. Chem.* **2000**, *275*, 34858−34866.
(42) Fridovich, I. *Science* **1978**, *201*, 875−880.
(43) Yusa, K.; Keiji, S. *Biochemistry* **1987**, *26*, 6684−6688.
(44) Adachi, S.; Nagano, S.; Watanabe, Y.; Ishimori, K.; Morishima, I. *Biochem. Biophys. Res. Commun.* **1991**, *180*, 138−144.
(45) Shimizu, N.; Kobayashi, K.; Hayashi, K. *J. Biochem.* **1988**, *104*, 136−140.
(46) Greer, J. *J. Mol. Biol.* **1971**, *59*, 107−126.
(47) Pulsinelli, P. D.; Perutz, M. F.; Nagel, R. L. *Proc. Natl. Acad. Sci. U.S.A.* **1973**, *70*, 3870−3874.
(48) Nagai, K.; Kagimoto, T.; Hayashi, A.; Taketa, F.; Kitagawa, T. *Biochemistry* **1983**, *22*, 1305−1311.
(49) Kanamori, D.; Yamada, Y.; Onoda, A.; Okamura, T.-a.; Adachi, S.; Yamamoto, H.; Ueyama, N. *Inorg. Chim. Acta* **2005**, *358*, 331−338.
(50) Ueyama, N.; Nishikawa, N.; Yamada, Y.; Okamura, T.-a.; Nakamura, A. *Inorg. Chim. Acta* **1998**, *283*, 91−97.
(51) Samanta, S.; Das, P. K.; Chatterjee, S.; Sengupta, K.; Mondal, B.; Dey, A. *Inorg. Chem.* **2013**, *52*, 12963−12971.
(52) Das, P. K.; Mittra, K.; Dey, A. *Chem. Commun.* **2013**, *50*, 5218−5220.
(53) Abe, M.; Kitagawa, T.; Kyogoku, Y. *J. Chem. Phys.* **1978**, *69*, 4526−4534.
(54) Argade, P. V.; Sassardi, M.; Rousseau, D. L.; Inubushi, T.; Ikeda-Saito, M.; Lapidot, A. *J. Am. Chem. Soc.* **1984**, *106*, 6593−6596.
(55) Li, X. Y.; Czernuszewicz, R. S.; Kincaid, J. R.; Su, Y. O.; Spiro, T. G. *J. Phys. Chem.* **1990**, *94*, 31−47.
(56) Dey, A.; Hocking, R. K.; Larsen, P.; Borovik, A. S.; Hodgson, K. O.; Hedman, B.; Solomon, E. I. *J. Am. Chem. Soc.* **2006**, *128*, 9825−9833.
(57) Dey, A.; Jenney, F. E.; Adams, M. W. W.; Johnson, M. K.; Hodgson, K. O.; Hedman, B.; Solomon, E. I. *J. Am. Chem. Soc.* **2007**, *129*, 12418−12431.
(58) Frisch, M. J.; et al. *Gaussian 03*, version C.02; Gaussian, Inc.: Wallingford, CT, 2004.
(59) Becke, A. D. *J. Chem. Phys.* **1993**, *98*, 5648−5652.
(60) Perdew, J. P. *Phys. Rev. B* **1986**, *33*, 8822−8824.
(61) Mulliken, R. S. *J. Chem. Phys.* **1955**, *23*, 1833−1840.
(62) Miertus, S.; Scrocco, E.; Tomasi, J. *Chem. Phys.* **1981**, *55*, 117−129.
(63) Torres, R. A.; Lovell, T.; Noodleman, L.; Case, D. A. *J. Am. Chem. Soc.* **2003**, *125*, 1923−1936.
(64) Taylor, C. P. S. *Biochim. Biophys. Acta* **1977**, *491*, 137−148.
(65) Walker, F. A. *Coord. Chem. Rev.* **1999**, *185*−*186*, 471−534.
(66) Jacob, G. S.; Orme-Johnson, W. H. *Biochemistry* **1979**, *18*, 2967−2975.
(67) Jacob, G. S.; Orme-Johnson, W. H. *Biochemistry* **1979**, *18*, 2975−2980.
(68) Burke, J. M.; Kincaid, J. R.; Peters, S.; Gagne, R. R.; Collman, J. P.; Spiro, T. G. *J. Am. Chem. Soc.* **1978**, *100*, 6083−6088.
(69) Chuang, W.-J.; Johnson, S.; Van Wart, H. E. *J. Inorg. Biochem.* **1988**, *34*, 201−219.
(70) Nagai, M.; Yoneyama, Y.; Kitagawa, T. *Biochemistry* **1989**, *28*, 2418−2422.
(71) Paulat, F.; Praneeth, V. K. K.; Näther, C.; Lehnert, N. *Inorg. Chem.* **2006**, *45*, 2835−2856.
(72) de Visser, S. P.; Tahsini, L.; Nam, W. *Chem.—Eur. J.* **2009**, *15*, 5577−5587.
(73) Green, M. T.; Dawson, J. H.; Gray, H. B. *Science* **2004**, *304*, 1653−1656.
(74) Behan, R. K.; Hoffart, L. M.; Stone, K. L.; Krebs, C.; Green, M. T. *J. Am. Chem. Soc.* **2006**, *128*, 11471−11474.
(75) Dey, A.; Jiang, Y.; Ortiz de Montellano, P.; Hodgson, K. O.; Hedman, B.; Solomon, E. I. *J. Am. Chem. Soc.* **2009**, *131*, 7869−7878.

(76) Kumar, D.; de Visser, S. P.; Sharma, P. K.; Derat, E.; Shaik, S. *JBIC, J. Biol. Inorg. Chem.* **2005**, *10*, 181−189.
(77) Jung, C. *Biochim. Biophys. Acta* **2011**, *1814*, 46−57.
(78) Zhang, Z.; Chouchane, S.; Magliozzo, R. S.; Rusling, J. F. *Anal. Chem.* **2002**, *74*, 163−170.
(79) Green, M. T.; Dawson, J. H.; Gray, H. B. *Science* **2004**, *304*, 1653−1656.